Macromolecules

Article

pubs.acs.org/Macromolecules

# Non-Equilibrium Dynamics of Vesicles and Micelles by Self-Assembly of Block Copolymers with Double Thermoresponsivity

Yu-Hang Tang,*[,†] Zhen Li,[†] Xuejin Li,[†] Mingge Deng,[†] and George Em Karniadakis*[,†,‡]

[†]Division of Applied Mathematics, Brown University, Providence, Rhode Island 02912, United States

[‡]Collaboratory on Mathematics for Mesoscopic Modeling of Materials, Pacific Northwest National Laboratory, Richland, Washington 99354, United States

Supporting Information

**ABSTRACT:** We present a mesoscopic simulation study of doubly thermoresponsive self-assemblies, revealing previously unknown dynamic behavior and proving experimental hypotheses. By explicitly modeling internal energy as a degree of freedom of coarse-grained particles, we simulated the thermally induced self-assembly process triggered by the evolution of temperature over time and space. We found that both external and intrinsic factors are responsible for altering the assembly pathway of thermoresponsive micelles and hence determining the final aggregate morphology. We identified a frequency regime where thermoresponsive unilamellar vesicles can sustain repeated heating−cooling cycles in a thermal loading test, and we quantified the collapse probability and half-life of the vesicles under frequencies that cause vesicle destruction. Two molecular movement modes dominate, namely flip and slip, in thermoresponsive bilayer membranes during the inversion of composition. We demonstrated that doubly thermoresponsive micelles and vesicles, as potential drug delivery vehicles, exhibit distinct hydrodynamic behavior when flowing through capillaries whose temperature spans across the inversion temperature of the carriers.

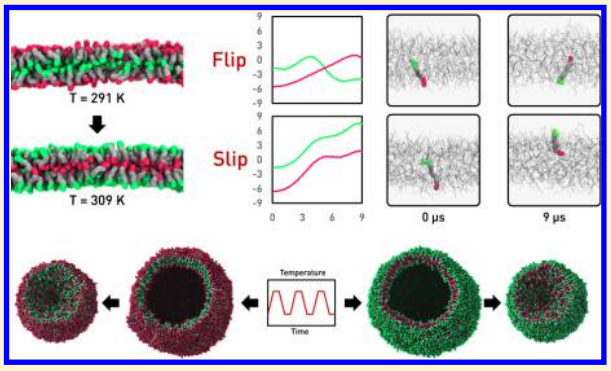


## 1. INTRODUCTION

Thermoresponsive polymers constitute a unique class of smart materials[1−3] that have received increasing attention due to their unique potential applications in fields such as drug delivery[4−9] and nanotechnology.[10−13] Above a certain critical temperature, a thermoresponsive polymer exhibits a sharp transition of solubility, manifested on the phase diagram either as an upper critical solution temperature (UCST) or a lower critical solution temperature (LCST). Simply put, a UCST polymer dissolves above its critical temperature, whereas an LCST polymer precipitates.

Akin to conventional amphiphilic copolymers,[14,15] copolymers with multiple thermoresponsive blocks[16−20] can form highly tunable self-assemblies which can be engineered for various applications.[21,22] While a quantitative understanding of the rich dynamic behavior of doubly thermoresponsive self-assemblies is vital for the efficient fabrication and utilization of these materials, experimental characterization can be laborious considering the vast parameter space generated by the combination of UCST/LCST behavior and transition temperature of each constituting block as well as environmental factors. In this paper, we present a study of the behavior of doubly thermoresponsive micelles and vesicles through computer simulations using a new energy-preserving dissipative particle dynamics (eDPD) model,[23−25] an extension of the classical dissipative particle dynamics (DPD) method.

DPD is a mesoscale particle simulation technique where each particle represents a cluster of atoms. A rigorous derivation of DPD from the Mori−Zwanzig formulation has been presented in a series of papers.[26−30] Among various molecular modeling techniques, DPD has been proven to be a powerful tool for mesoscopic modeling of soft matter due to its capability in reproducing both static and dynamic properties of the system.[31,32] The classical DPD formulation integrates a built-in pairwise thermostat that effectively maintains the system temperature at a target value. Being a valuable feature for most simulation scenarios that require isothermal conditions, this thermostat turns out to be an obstacle for studying temperature-related phenomena. The eDPD formulation allows us to overcome this limitation by modeling (at a coarse-grained molecular level) internal energy as a degree of freedom of the particles and therefore to calculate temperature-dependent pairwise interaction parameters on a per-particle basis. This capability allows us to model the *transient* and *local* behavior of thermoresponsive block copolymers under different heating rates and in flow fields with uneven temperature distribution. The eDPD formulation, together with auxiliary functionalities,

**Received:** February 19, 2016
**Revised:** March 21, 2016
**Published:** April 1, 2016





DOI: 10.1021/acs.macromol.6b00365
*Macromolecules* 2016, 49, 2895−2903

was implemented into the GPU-accelerated LAMMPS package USERMESO.[24]

## 2. METHOD

Our eDPD method[23] extends the original DPD framework[33] by explicitly modeling each particle's internal energy as a degree of freedom:

$$\frac{d\mathbf{r}_i}{dt} = \mathbf{v}_i \tag{1}$$

$$m\frac{d\mathbf{v}_i}{dt} = \mathbf{f}_i = \sum_{i\neq j}(\mathbf{F}_{ij}^C + \mathbf{F}_{ij}^D + \mathbf{F}_{ij}^R) \tag{2}$$

$$C_v\frac{dT_i}{dt} = q_i = \sum_{i\neq j}(Q_{ij}^C + Q_{ij}^V + Q_{ij}^R) \tag{3}$$

where $t$, $\mathbf{r}_i$, $\mathbf{v}_i$, $\mathbf{f}_i$, $m_i$, $T_i$, $q_i$, and $C_v$ denote time, position, velocity, force, mass, temperature, heat flux, and heat capacity of DPD particles.

The force $\mathbf{f}_i$ acting on each particle consists of three pairwise-additive components, i.e., a conservative one, a dissipative one, and a random one:

$$\mathbf{F}_{ij}^C = a_{ij}(T_{ij})w_C(r_{ij})\mathbf{e}_{ij} \tag{4}$$

$$\mathbf{F}_{ij}^D = -\gamma_{ij}w_D(r_{ij})(\mathbf{e}_{ij}\cdot\mathbf{v}_{ij})\mathbf{e}_{ij} \tag{5}$$

$$\mathbf{F}_{ij}^R = \sigma_{ij}w_R(r_{ij})\xi_{ij}\delta t^{-1/2}\mathbf{e}_{ij} \tag{6}$$

Here $T_{ij} = (T_i + T_j)/2$ is the pairwise local temperature between particle $i$ and $j$. A common choice for the pairwise repulsive force coefficient $a_{ij}(T_{ij})$ that reproduces the compressibility of water is

$$a_{ij}(T_{ij}) = \frac{75k_BT_{ij}}{\rho} \tag{7}$$

The noise level $\sigma_{ij}$ and the pairwise friction coefficient $\gamma_{ij}$ are related to each other through the fluctuation−dissipation theorem:[34]

$$\sigma_{ij} = \sqrt{2\gamma_{ij}k_BT_{ij}} \tag{8}$$

The pairwise heat flux also consists of three components:

$$Q_{ij}^C = k_{ij}w_{CT}(r_{ij})\left(\frac{1}{T_i} - \frac{1}{T_j}\right) \tag{9}$$

$$Q_{ij}^V = \frac{1}{2C_v}\{w_D(r_{ij})[\gamma_{ij}(\mathbf{e}_{ij}\cdot\mathbf{v}_{ij})^2 - \sigma_{ij}^2/m] - \sigma_{ij}w_R(r_{ij})(\mathbf{e}_{ij}\cdot\mathbf{v}_{ij})\xi_{ij}\delta t^{-1/2}\} \tag{10}$$

$$Q_{ij}^R = \beta_{ij}w_{RT}(r_{ij})\zeta_{ij}\delta t^{-1/2} \tag{11}$$

while the contact heat flux coefficient $k_{ij}$ and random heat flux level $\beta_{ij}$ can be determined as

$$k_{ij} = \frac{C_v^2\kappa(T_i + T_j)^2}{4k_B} \tag{12}$$

$$\beta_{ij} = 2k_Bk_{ij} \tag{13}$$

The following weight functions were used in this study for forces and heat fluxes:

$$w_R(r_{ij}) = w_C(r_{ij}) = w_{RT}(r_{ij}) = \left(1 - \frac{|r_{ij}|}{r_c}\right) \tag{14}$$

$$w_D(r_{ij}) = w_{CT}(r_{ij}) = w_R^2(r_{ij}) \tag{15}$$

The affinity between different types of DPD particles is controlled by the conservative force coefficients $a_{ij}$. A value bigger than the reference value $a_{ij}^* \doteq 75\ k_B\ T/\rho$ indicates that the particles are immiscible, while a smaller value indicates good compatibility. In order to reproduce the temperature-dependent behavior of LCST and UCST polymers, we set the excess repulsion $\delta a_{ij} \doteq a_{ij} - a_{ij}^*$ to be a sigmoidal function of $T$:[25]

$$\delta a_{ij} = \frac{\delta a_{ij}^0}{1 + \exp[\omega(T_{ij} - T_0)]} \tag{16}$$

As visualized in Figure 1, $\delta a_{ij}^0$ defines the maximum excess repulsion, while negative and positive values of $\omega$ give rise to LCST and UCST behaviors, respectively. The magnitude of $\omega$ determines the sharpness of the transition.The complete form of the temperature-dependent conservative force coefficients therefore becomes

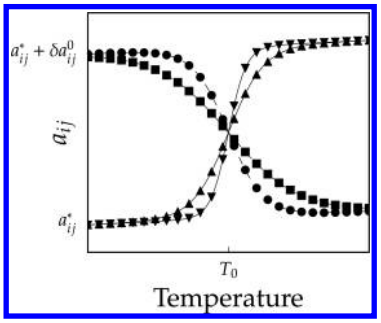


**Figure 1.** Pairwise repulsive coefficient $a_{ij}$ as a function of temperature as determined by eq 17.

$$a_{ij}(T_{ij}) = \frac{75k_BT_{ij}}{\rho} + \frac{\delta a_{ij}^0}{1 + \exp[\omega(T_{ij} - T_0)]} \tag{17}$$

We carried out the simulations in reduced units. The dimensionless temperature $T$, length $L$ and mass $m$ are scaled from their physical counterparts $T^*$, $L^*$, and $m^*$ with a reference scale $T_0 = 300$ K, $L_0 = 2.99$ nm, and $m_0 = 4000$ Da:[23]

$$T \doteq \frac{T^*}{T_0} = \frac{T^*}{300\ \text{K}}, \quad L \doteq \frac{L^*}{L_0} = \frac{L^*}{2.99\ \text{nm}}, \quad m \doteq \frac{m^*}{m_0} = \frac{m^*}{4000\ \text{Da}} \tag{18}$$

where $m_0$ is determined using the density of water and a DPD particle number density $\rho_n = 4$.

The measured diffusivity $D^P$ of the solvent beads, each representing 222 water molecules ($N_w = 222$), is 0.305 in the dimensionless units. By connecting this to the experimental self-diffusivity of water $D^W = 2.43 \times 10^{-9}$ m$^2$/s, the time scale can be determined as[35]



DOI: 10.1021/acs.macromol.6b00365
Macromolecules 2016, 49, 2895−2903

$$\tau = \frac{N_w \times D^P \times {L_0}^2}{D^W} = \frac{222 \times 0.305 \times (2.99 \times 10^{-9}\ \mathrm{m})^2}{2.43 \times 10^{-9}\ \mathrm{m^2 \cdot s^{-1}}} \approx 250\ \mathrm{ns} \quad (19)$$

A time step size of $\delta t = 0.01\ \tau$ was used throughout the study.

To verify the ability of our proposed eDPD model in reproducing the temperature-induced conformational variation of thermoresponsive polymers near the $\theta$ temperature, we plot the time-averaged per-monomer radius of gyration $\left\langle \frac{R_g^2}{N} \right\rangle$ of a single polymer chain versus temperature and contour length as obtained from ensemble-averaged equilibrium eDPD simulations. With $a_{ij}^{*} = 10.0$, $\delta a_{ij}^{0} = 27.5$, $\omega = 100$, we observe the lines for different chain length converge at the $\theta$ temperature as shown in Figure 2A. This is in qualitative agreement with ref.[36,37] as in Figure 2B.

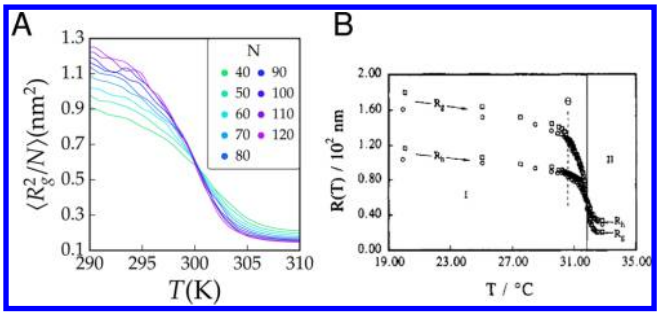


**Figure 2.** (A) Temperature dependence of the conformation of single polymer chains reproduced by the eDPD model. (B) Radius of gyration and hydrodynamic radius of Poly(*N*-isopropylacrylamide) single chain observed by light scattering experiments. Reprinted with permission from ref 36 Copyright 1995 American Chemical Society.

Detailed simulation setup for each specific system can be found in the Supporting Information.

## 3. RESULTS AND DISCUSSION

**3.1. Thermoresponsive Micelles.** Consider the behavior of micelles formed by a LCST-UCST diblock copolymer upon heating and denote by $\theta^L$ and $\theta^U$ the critical temperature of the LCST and UCST blocks, respectively. Given a temperature range of $[T_0, T_1]$ that the system may experience, the combination of LCST and UCST behavior and the relative difference between $\theta^L$, $\theta^U$, $T_0$ and $T_1$ gives rise to five possible cases of thermally induced assembly as revealed by our eDPD simulations and summarized in Table 1. In case A, the LCST block and the UCST block share the same critical temperature. In this case, an *inversion* of the micellar core−shell structure was observed upon heating from below the critical temperature to above due to an interchange of solvent affinity of the polymer blocks. In case B, the UCST block has a critical temperature above the highest temperature simulated and hence was always hydrophobic during the simulation. In this case, the polymers formed micelles at low temperature but Janus-like globular aggregates at high temperature as the LCST block lost hydrophilicity upon heating. In case C, the LCST block has a critical temperature below the lowest temperature accessible by the simulation and therefore was always hydrophobic. In this case, the polymers formed hydrophobic globular aggregates at low temperature but micelles at high temperature as the UCST block gained hydrophilicity upon heating. Cases B and C can be effectively viewed as the first and second half of the process in case A. In case D, the UCST critical temperature is low enough to render the UCST blocks constantly hydrophilic. The polymers assembled into micelles from a uniform dispersion as the LCST block lost hydrophilicity upon heating. Case E is

**Table 1. Five Thermally Induced Assembly Scenarios Leading to Fundamentally Different Structure**[a]

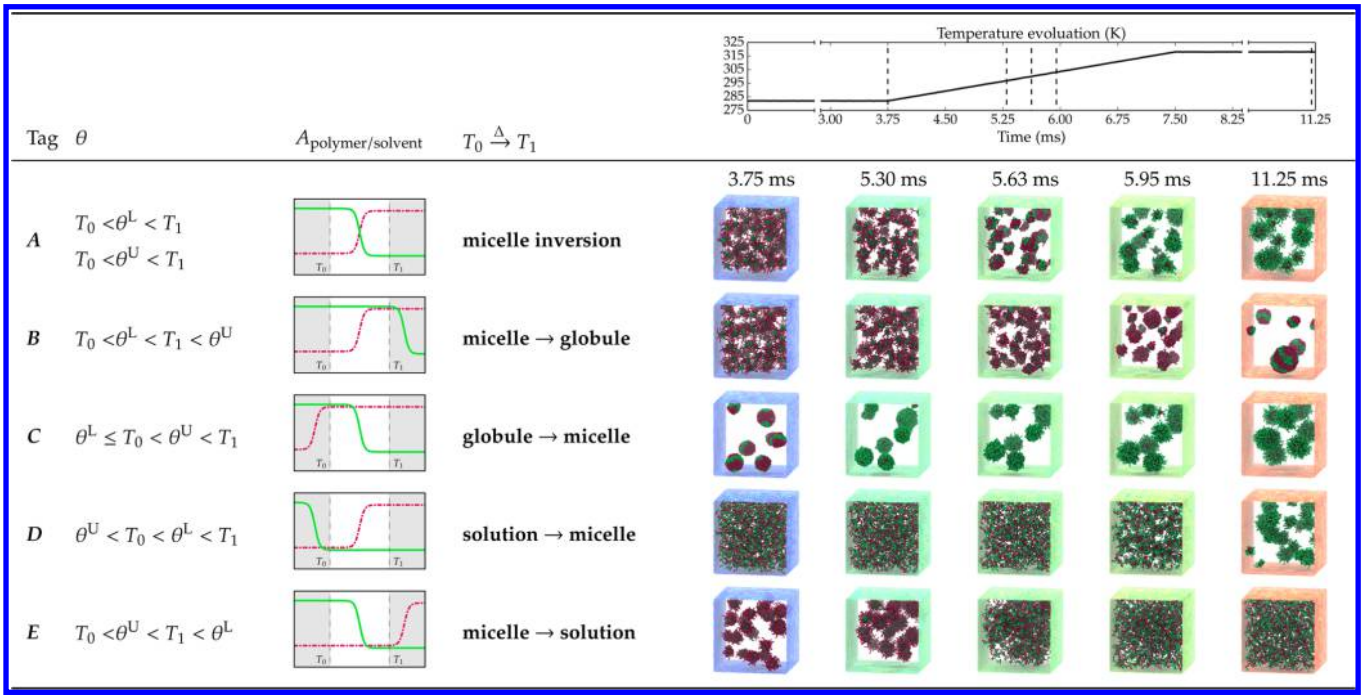


[a]A label is assigned to each scenario for later discussion. Snapshots of the systems over the heating process are given in the last column. LCST and UCST blocks are in red dashed and green solid lines, respectively. Background colors of the simulation boxes indicate temperature ranging from 288 (blue) to 312 K (red).



DOI: 10.1021/acs.macromol.6b00365
*Macromolecules* 2016, 49, 2895−2903

simply the inverse of case D. Cases D and E can be regarded as the process of drug loading and unloading into/from the hydrophobic core of the micelles, respectively.

Given the nonequilibrium nature of the inversion of thermoresponsive micelles, it is natural to expect that the process can be controlled by adjusting the rate at which solvent affinity changes.[38] To probe this, we simulated case A again with two replicas from exactly the same initial configuration. The first replica underwent a smooth heating procedure, while the second one experienced a sharp temperature jump. In the first replica, large aggregates formed via the fusion of smaller ones at around $T$ = 300 K, i.e., the $\theta$ temperature of the blocks. These aggregates eventually formed large spherical micelles as visualized in Figure 3A. In the second replica, fast heating quickly generated large numbers of small micelles with a narrower size distribution as illustrated by Figure 3B. Therefore, it is possible to use the *heating rate* to tune the size distribution of thermoresponsive micelles.[39]

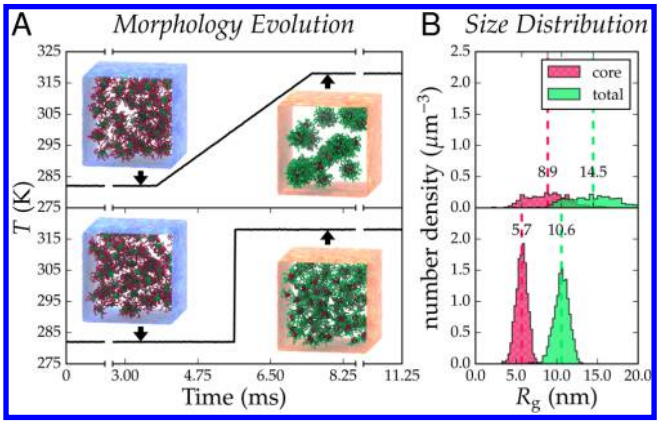


**Figure 3.** Fast heating gives rise to smaller micelles with a sharper size distribution: (A) morphological change of micelles in fast and slow heating; (B) size distribution of the micelles after inversion.

The critical temperature, as an intrinsic property of the polymers, also significantly affects the inversion dynamics. The difference $\Delta\theta \doteq \theta^{U} - \theta^{L}$ between the critical temperatures of the blocks in a copolymer is more informative than the absolute values because the latter can be always tuned with respect to a target temperature.[40,41] Therefore, we simulated UCST−LCST diblock copolymers of different $\Delta\theta$ subjected to a gradual heating process and characterized the process in Figure 4 using direct visualization and the average radius of gyration $R_g$ of the polymers.

Large positive $\Delta\theta$, as shown in Figure 4A, yielded V-shaped $R_g$ curves with a deep valley followed by a high plateau. A max-min difference of up to ∼0.83 nm indicates that the polymer chains deformed significantly at intermediate temperatures. The reason is that the LCST blocks lost hydrophilicity quite early at a low temperature, while the UCST blocks only became hydrophilic at a relatively high temperature. As a result neither block was soluble at intermediate temperatures. This led to large chain deformations during the consequent aggregate formation and fusion process. An overall increase of ∼0.35 nm in $R_g$ was observed at the end of the process. This is mostly contributed by the LCST blocks whose $R_g$ increased by ∼0.4 nm as shown in Figure 4B. Meanwhile the $R_g$ of the UCST blocks slightly decreased by ∼0.05 nm.

If $\Delta\theta$ is negative or close to zero, the $R_g$ curves are W-shaped with two shallow minima as shown in Figure 4A. The two minima correspond to the solvation of the UCST blocks and the precipitation of the LCST blocks. The solvation events happened before the precipitation, resulting in an intermediate state of fully dispersed polymer solution. This may result in a thorough release of the payload due to the complete

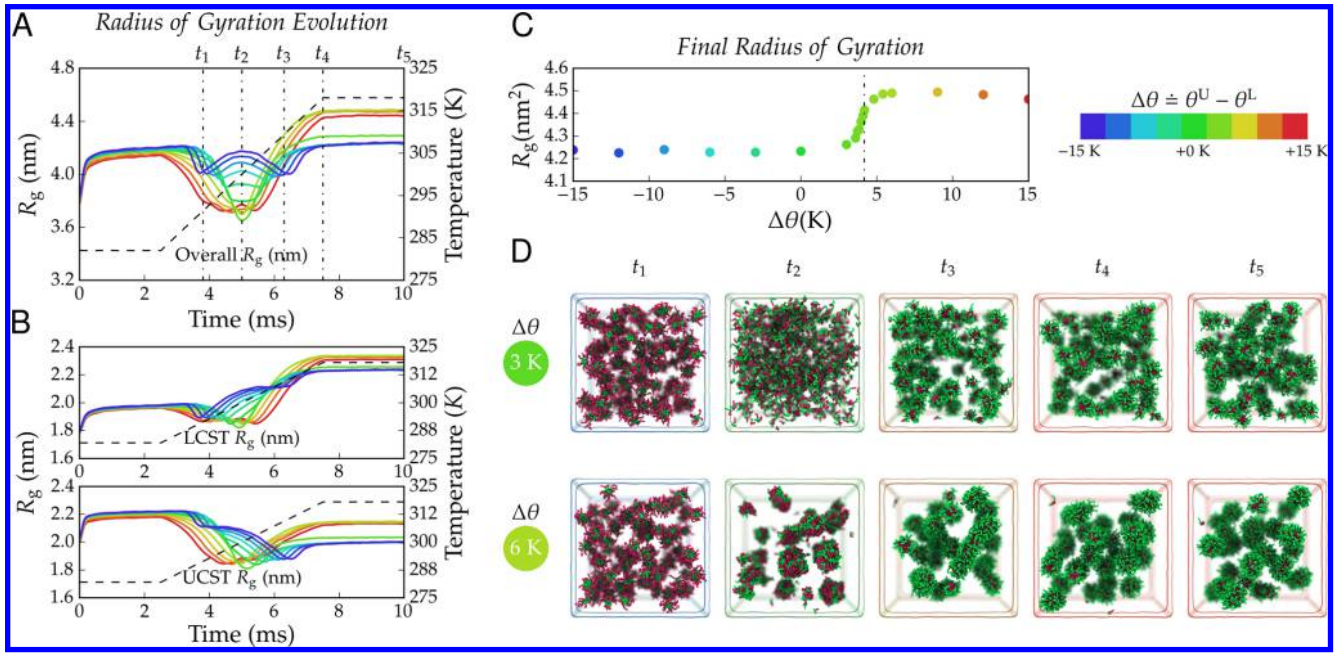


**Figure 4.** Two slow-inversion pathways, i.e. disintegration-reintegration and aggregation-fission, exist depending on the critical temperature of the LCST (red) and UCST (green) blocks. (A and B) average radius of gyration ($R_g$) of LCST−UCST molecules of different $\Delta\theta$ during the slow inversion. (C) A jump in the final average radius of gyration of the micelles versus the separation indicates a high sensitivity between the LCST and UCST $\theta$ temperature and the pathway taken. (D) Snapshots of the micellar systems during the inversion process for $\Delta\theta$ = 3 and 6 K.



DOI: 10.1021/acs.macromol.6b00365
*Macromolecules* 2016, 49, 2895−2903

disassembly of thermoresponsive micelles. The change in average $R_g$ after the inversion is negligible because the increase of the LCST blocks is canceled by the decrease of the UCST blocks as shown by Figure 4B. The average size of the obtained micelles is small and similar to those formed in the fast heating scenario, because no aggregate formation or fusion process occurred.

We observed that the final average $R_g$ of the polymers is highly sensitive to $\Delta\theta$ as indicated in Figure 4C. A bisection search revealed the existence of a critical temperature $\Delta\theta_c$ = 4.08 K, around which a slight difference in $\Delta\theta$ could result in a sharp change in $R_g$. This can be considered together with a direct visualization of the micellar morphology evolution for $\Delta\theta$ = 3 and 6 K as given in Figure 4D. A disintegration-reintegration process occurred when $\Delta\theta$ = 3 K, while an aggregation-fission process occurred instead when $\Delta\theta$ = 6 K, where toroidal micellar intermediates formed and eventually broke down into spherical micelles. It is the alteration between the disintegration-reintegration and the aggregation-fission pathway that gives rise to this sensitive response of $R_g$ with respect to $\Delta\theta$. We also note that a sharp temperature jump always direct the system into the disintegration-aggregation pathway irrespective of $\Delta\theta$.

**3.2. Thermoresponsive Vesicles.** Under certain conditions, a unilamellar vesicle (ULV) formed by a $L_2N_5U_2$ triblock copolymer may invert by switching its surface and internal thermoresponsive blocks reversibly as shown in Figure 5A. The L and U blocks are LCST and UCST, respectively, while the N blocks are nonresponsive hydrophobic blocks. The evolution of the radial density distribution $\rho(r)$ for each type of polymer blocks during one inversion is given in Figure 5B. An interchange of the shapes of LCST and UCST density distribution is observed. The peaks of the curves raised or lowered vertically over time instead of shifting horizontally, while the density distribution of the nonresponsive blocks only displayed minor change. This indicates that the molecules did not invert collectively in a lock-step fashion but rather by diffusing through the wall formed by the nonresponsive blocks.

The collapse and subsequent release of the containing fluid of a vesicle is a stochastic event due to the metastable nature of ULVs,[42] and is critical in designing vesicle-based drug carriers. To quantify this behavior, a thermal loading test was performed in which 576 ensembles each containing a single ULV were subjected to repeated heating−cooling cycles of frequencies ranging between 5 $\mu$s/cycle and 1.25 ms/cycle. As shown in Figure 5C, both very high and low thermal loading frequencies eventually led to the collapse of the vesicles in all ensembles. For these cases the collapse probability distribution parameters, mean survival time, and half-life were estimated and given in Table 2. The disruption of vesicle structure under the 5 and 12.5 $\mu$s/cycle loading frequencies can be attributed to the constant changing of hydrophilicity of the thermoresponsive blocks at a pace faster than that of a complete inversion. The collapse of vesicles at very low frequencies is likely a consequence of the system staying too long near the $\theta$ temperature, where both thermoresponsive blocks were weakly hydrophobic. At intermediate frequencies, however, up to 50−70% of the vesicles can survive for a long time after a short knockout phase which destroyed the less stable ones.

**3.3. Molecular Mechanism of Thermally Induced Inversion.** An intriguing question arises concerning how an individual molecule behaves during thermally induced inversion to accomplish the switching of overall composition in thermoresponsive self-assemblies.[43] To answer the question, we employed the proper orthogonal decomposition (POD)

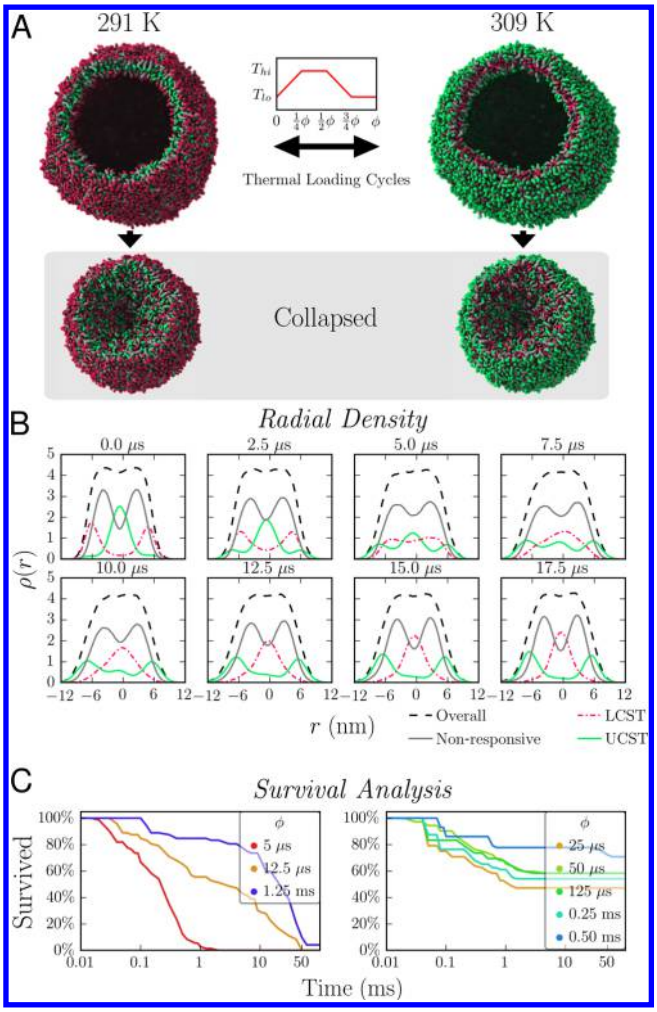


**Figure 5.** Thermoresponsive vesicles invert by diffusion and respond differently to various thermal loading frequencies. (A) A vesicle formed by $L_2N_5U_2$ thermoresponsive block copolymer can invert repeatedly when subjected to thermal loading cycles and may collapse irreversibly. (B) Radial density distributions of polymer blocks during one inversion. (C) At both high and low frequencies, vesicles collapse completely, but at intermediate frequencies many vesicles can survive for a long time. LCST, UCST, and nonresponsive blocks are shown by red dashes, green solids, and gray, respectively.

**Table 2. Survival Rates and Estimated Collapse Probability of Vesicles under Different Thermal Loading Frequencies**[a]

| | | $p(t;a,b) = [t^{a-1}/\Gamma(a)b^a]e^{-t/b}$ | | | |
|---|---|---|---|---|---|
| period | survived (%) | $a$ | $b$ | mean lifetime (ms) | half-life (ms) |
| 5 $\mu$s | 0.0 | 1.170 | 0.239 | 0.28 | 0.21 |
| 12.5 $\mu$s | 0.0 | 0.394 | 23.10 | 9.11 | 3.25 |
| 25 $\mu$s | 47.2 | * | * | * | * |
| 50 $\mu$s | 58.3 | * | * | * | * |
| 125 $\mu$s | 58.3 | * | * | * | * |
| 0.25 ms | 54.2 | * | * | * | * |
| 0.50 ms | 70.8 | * | * | * | * |
| 1.25 ms | 4.2 | 0.461 | 29.07 | 20.36 | 8.59 |

[a]An asterisk indicates a field that cannot be estimated reliably due to the long tail of the failure probability.



DOI: 10.1021/acs.macromol.6b00365
Macromolecules 2016, 49, 2895−2903

method to extract patterns, or *modes*, from noisy molecular trajectories.

A membrane in periodic space, as displayed in Figure 6B, was used as a zoomed-in model for studying the motion of

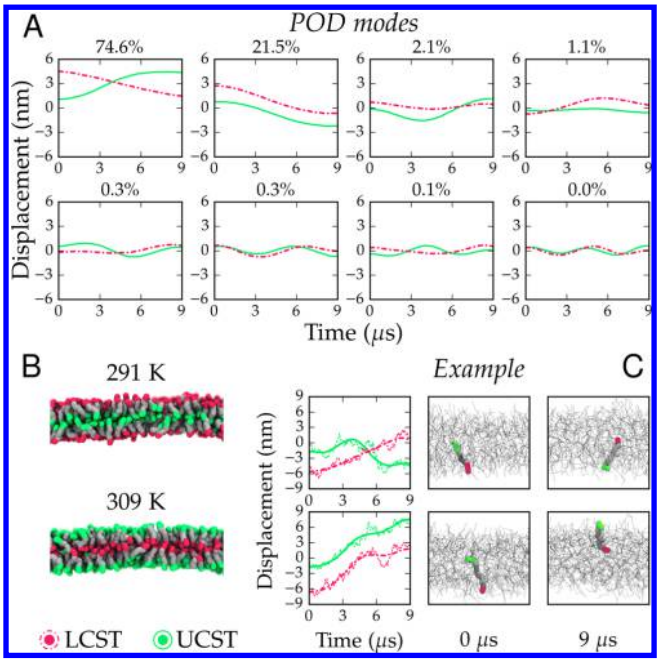


**Figure 6.** POD analysis reveals two dominant molecular movement modes, i.e., flip and slip, during membrane inversion. (A) POD modes of UCST and LCST block trajectories during membrane inversion. (B) Bilayer membrane formed by the $L_2$ $N_5$ $U_2$ thermoresponsive block copolymer. (C) Examples of molecules following the *flip* and *slip* modes (see also Supporting Information, Video 1 and Video 2); surrounding molecules are rendered as gray lines. Dashed lines represent exact trajectories, while solid lines are smoothed versions of the trajectories reconstructed from the eight most energetic POD modes. LCST, UCST, and nonresponsive blocks are colored in red dashes, green solids, and gray, respectively.

individual chains in a vesicle during thermally induced inversion. The first eight most energetic POD modes are shown in Figure 6A, where the red and green lines correspond to the trajectories of the UCST and LCST block in the direction perpendicular to the membrane. The modes are captioned by the percentage of molecules that belonged to the mode as classified using a nearest-neighbor algorithm under cosine similarity (see Supporting Information for details of the POD analysis). The two dominant modes, combined with examples as given in Figure 6C, can be interpreted as such: 1) in the first mode, the trajectories of LCST and UCST blocks cross once, thus indicating that the molecule *flips* during the process; 2) in the second mode, the two trajectories move from above zero to below in parallel, indicating the molecule *slips* from one leaflet of the membrane into the other one without rotation. The other modes represent higher frequency oscillations due to the stochastic nature of the molecular movement. Surprisingly, 21.5% of the molecules in fact assumed the *slip* mode and hence did not invert orientation although the membrane inverted its overall composition. This exchange rate is significantly higher than the spontaneous flip-flop rate between leaflets of lipid membranes[44] and may be used as a means of cross-membrane signaling for thermoresponsive polymersomes.

**3.4. Thermoresponsive Self-Assemblies in Flow.** The dynamics of self-assemblies in flow is an important concern in designing thermoresponsive drug delivery systems. After injection and propagation in the patient's circulatory system, thermoresponsive drug carriers will eventually reach the capillaries at the target site where they release the payload in response to local thermal conditions.[6] At this scale, the two-phase nature of blood dominates and results in the concentration of most drug carriers in a cell-free layer (CFL)[45,46] of ca. 1−2 $\mu$m in thickness for hematocrit level at 45%.[47,48] To emulate this condition and probe the dynamics of thermoresponsive carriers in the CFL, we simulated micelles and vesicles in a periodic cylindrical tube of length $l$ = 800 nm and radius $r$ = 60 nm. The first half of the tube wall was heated up above the transition temperature of the polymer blocks, while the second half was cooled down below the transition temperature. A pressure gradient was applied to drive the carriers to flow through the two regions of different temperature.

As Figure 7A demonstrates, a micelle formed by one LCST block and one hydrophilic block disintegrated completely after

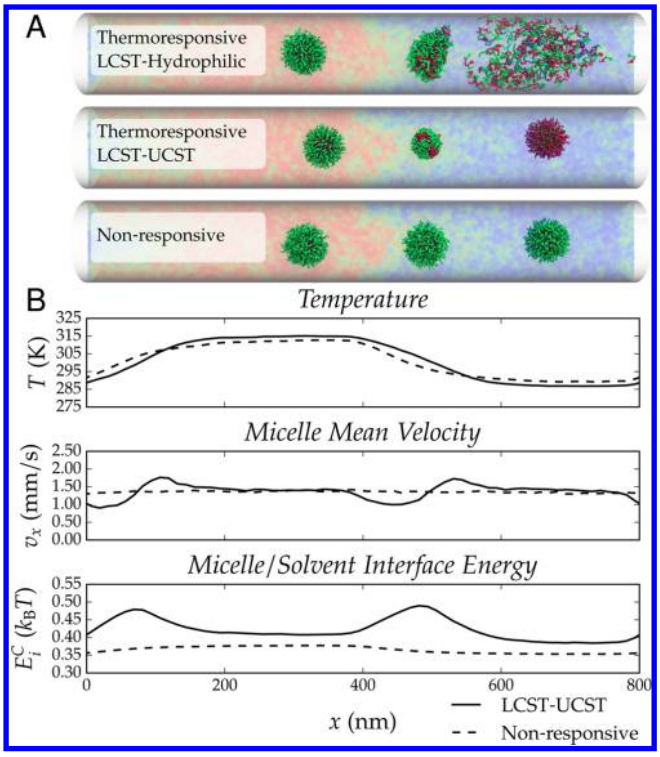


**Figure 7.** Thermoresponsive micelles experienced deformation and resistance when traveling through thermal interfaces while a nonresponsive micelle was not affected (see also Supporting Information, Video 3). (A) Top: snapshots of a LCST-hydrophilic micelle in the tube at 0.19, 0.32, and 0.46 ms. **Middle**: Snapshots of a LCST-UCST micelle in the tube at 0.21, 0.34, and 0.46 ms. Bottom: snapshots of a nonresponsive micelle in the tube at 0.19, 0.31, and 0.44 ms. (B) Mean temperature, lateral velocity, and solvent interaction energy of the micelle along the tube.

crossing the thermal interface, while a LCST-UCST micelle underwent shape transformations each time it crossed the boundary between the two temperature zones. The release of payload molecules or nanoparticles can be achieved in both cases as a result of the exposure of the original micellar cores. In addition, the LCST-UCST micelle tended to slow down while


DOI: 10.1021/acs.macromol.6b00365
*Macromolecules* 2016, 49, 2895−2903

approaching the interface but accelerate afterward due to the surface energy change associated with the temperature jump as quantified by Figure 7B. By contrast, a nonresponsive micelle did not exhibit this type of behavior. It remained stable and traveled at almost constant velocity along the tube and eventually outran the LCST-UCST micelle after several cycles. Diffusion through the hydrophobic core is the major approach of payload releasing for this nonresponsive micelle due to its structural stability.

A vesicle assembled by nonresponsive amphiphilic polymers, as shown in Figure 8A, remained intact after traveling through

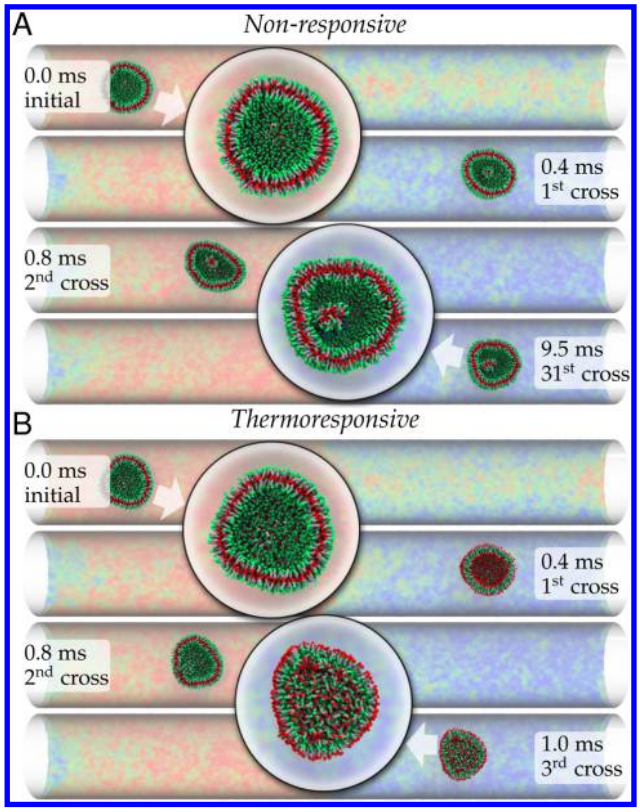


**Figure 8.** (A) A nonresponsive vesicle can sustain a long time, while (B) a thermoresponsive one deformed and released its enclosed fluid after crossing thermal interfaces a few times. Background colors indicate temperatures ranging from 288 (blue) to 312 K (red).

thermal interfaces for more than 30 times, while a thermoresponsive vesicle collapsed and lost its containing fluid after crossing thermal interfaces for the third time as shown in Figure 8B. A 200-ensemble simulation showed that on average a thermoresponsive vesicle can cross thermal interfaces for 2.24 ± 1.24 (SD) times before collapsing.

**3.5. Related Work.** Self-assemblies formed by thermoresponsive copolymers have been observed experimentally to switch their inside and outside blocks following a change in ambient temperature.[43] However, there is a lack of details on how the inversion proceeds in terms of the dynamics of individual polymer chains. In absence of direct data on the inversion dynamics of *thermoresponsive* polymers, we consider experimental work reporting the morphology and inversion dynamics of pH-sensitive polymer aggregates as a close analogue for comparing against our simulation results. Wang et al.[49] examined the inversion dynamics of micelles formed by PVBA−PMEMA diblock copolymers using a stopped-flow apparatus with light scattering detector. They found that the inversion from VBA−core to MEMA−core follows a fusion-disintegration-reintegration pathway, while the inversion from MEMA−core to VBA−core proceeds by micelle splitting. Similar events can be found in Figure 4 but in a different ordering of the events. Liu and Eisenberg[50] studied the inversion dynamics of vesicles formed by PAA−PS-P4VP triblock copolymers and postulated that the inversion involves the diffusion of polymer chains through a softened wall but did not provide evidence. We provide a systematic and quantitative evidence for this as shown in Figure 5, which characterizes the evolution of block density distribution, as well as the molecular movement modes analysis as detailed in section 3.3.

The classical DPD method has been used for the study of various thermoresponsive polymer systems such as micelles,[51] self-regenerating gels,[52] multilayered polymersomes formed by asymmetric thermoresponsive brushes,[53] and model liposomes.[54] However, in these studies, the interaction between the thermoresponsive polymer and solvent is either defined as a function of the global system temperature $T$ or simply adjusted manually at a given point during the simulation to mimic the thermoresponsive effect. This is an artificial consequence of the pairwise thermostat of the classical DPD method which constraints the system in an isothermal state. As a result only equilibrium properties or dynamic processes incurred by an infinitely sharp temperature jump can be reliably studied. In our eDPD model, however, the pairwise repulsion only depends on the local temperature $T_i$ and $T_j$ of the two interacting particles and hence allows the study of nonisothermal processes and systems.

## 4. CONCLUSION

We have performed systematic mesoscopic simulations to elucidate the molecular mechanisms and quantified the dynamics of self-assemblies formed by doubly thermoresponsive block copolymers. We simulated several scenarios of micelle formation and destruction, and examined factors that affect the inversion process of micelles of dual thermoresponsivity. We discovered two different micelle inversion pathways during slow temperature change depending on the solubility of the polymers at intermediate temperatures. We identified a frequency regime where thermoresponsive unilamellar vesicles can invert reversibly in repeated thermal loading cycles and quantified the failure probability of the vesicles under frequencies that cause instability. We found that thermoresponsive bilayer membranes exhibit a very high ratio of molecular migration between the two leaflets during thermally induced inversion. Simulations of micelles in a small vessel revealed the unique behavior of thermoresponsive micelles in flow fields with uneven temperature distribution. We discovered some surprising mesoscopic molecular behavior and provided new evidence for theoretical hypotheses. Our work demonstrated the capability and potential of mesoscopic computer simulation in assisting and accelerating the design and optimization of complex self-assembly structures consisting of thermoresponsive polymers.

## ■ ASSOCIATED CONTENT

### Supporting Information

The Supporting Information is available free of charge on the ACS Publications website at DOI: 10.1021/acs.macromol.6b00365.



DOI: 10.1021/acs.macromol.6b00365
*Macromolecules* 2016, 49, 2895−2903

Details of simulation (PDF)
Slip mode (AVI)
Flip mode (AVI)
Deformation and resistance of micelles (PDF)

## AUTHOR INFORMATION


### Corresponding Authors

*(Y.-H.T.) E-mail: yuhang_tang@brown.edu.
*(G.-E.K.) E-mail: george_karniadakis@brown.edu.


### Notes

The authors declare no competing financial interest.

## ACKNOWLEDGMENTS

This work was supported by the Department of Energy (DOE) Collaboratory on Mathematics for Mesoscopic Modeling of Materials (CM4). Simulations were carried out at the Oak Ridge Leadership Computing Facility through the Innovative and Novel Computational Impact on Theory and Experiment program at Oak Ridge National Laboratory under Projects BIP102 and BIP118. Y.-H.T. thanks Changho Kim for discussions on polymer diffusivity. Y.-H.T. acknowledges partial financial support from an IBM Ph.D. Scholarship Award.

## REFERENCES


(1) Jochum, F. D.; Theato, P. Temperature-and light-responsive smart polymer materials. *Chem. Soc. Rev.* **2013**, *42* (17), 7468−7483.
(2) Roy, D.; Brooks, W. L. A.; Sumerlin, B. S. New directions in thermoresponsive polymers. *Chem. Soc. Rev.* **2013**, *42* (17), 7214−7243.
(3) Elsabahy, M.; Wooley, K. L. Design of polymeric nanoparticles for biomedical delivery applications. *Chem. Soc. Rev.* **2012**, *41* (7), 2545−2561.
(4) Mai, W.; Sun, B.; Chen, L.; Xu, F.; Liu, H.; Liang, Y.; Fu, R.; Wu, D.; Matyjaszewski, K. Water-dispersible, responsive, and carbonizable hairy microporous polymeric nanospheres. *J. Am. Chem. Soc.* **2015**, *137* (41), 13256−13259.
(5) Siegel, R. A. Stimuli sensitive polymers and self regulated drug delivery systems: a very partial review. *J. Controlled Release* **2014**, *190*, 337−351.
(6) Kashyap, S.; Jayakannan, M. Thermo-responsive and shape transformable amphiphilic scaffolds for loading and delivering anticancer drugs. *J. Mater. Chem. B* **2014**, *2* (26), 4142−4152.
(7) Kost, J.; Langer, R. Responsive polymeric delivery systems. *Adv. Drug Delivery Rev.* **2012**, *64*, 327−341.
(8) Timko, B. P.; Arruebo, M.; Shankarappa, S. A.; McAlvin, J. B.; Okonkwo, O. S.; Mizrahi, B.; Stefanescu, C. F.; Gomez, L.; Zhu, J.; Zhu, A.; Santamaria, J.; Langer, R.; Kohane, D. S. Near-infrared-actuated devices for remotely controlled drug delivery. *Proc. Natl. Acad. Sci. U. S. A.* **2014**, *111* (4), 1349−1354.
(9) Zhang, Z.; Wang, J.; Nie, X.; Wen, T.; Ji, Y.; Wu, X.; Zhao, Y.; Chen, C. Near infrared laser-induced targeted cancer therapy using thermoresponsive polymer encapsulated gold nanorods. *J. Am. Chem. Soc.* **2014**, *136* (20), 7317−7326.
(10) Kolodziej, C. M.; Maynard, H. D. Shape-shifting micro-and nanopatterns controlled by temperature. *J. Am. Chem. Soc.* **2012**, *134* (30), 12386−12389.
(11) Ward, M. A.; Georgiou, T. K. Thermoresponsive terpolymers based on methacrylate monomers: Effect of architecture and composition. *J. Polym. Sci., Part A: Polym. Chem.* **2010**, *48* (4), 775−783.
(12) Reed, J. A.; Lucero, A. E.; Hu, S.; Ista, L. K.; Bore, M. T.; López, G. P.; Canavan, H. E. A low-cost, rapid deposition method for smart films: applications in mammalian cell release. *ACS Appl. Mater. Interfaces* **2010**, *2* (4), 1048−1051.
(13) Varghese, V. M.; Raj, V.; Sreenivasan, K.; Kumary, T. V. In vitro cytocompatibility evaluation of a thermoresponsive nipaam-mma copolymeric surface using l929 cells. *J. Mater. Sci.: Mater. Med.* **2010**, *21* (5), 1631−1639.
(14) Zhang, Z.; Marson, R. L.; Ge, Z.; Glotzer, S. C.; Ma, P. X. Simultaneous nano- and microscale control of nanofibrous microspheres self-assembled from star-shaped polymers. *Adv. Mater.* **2015**, *27* (26), 3947−3952.
(15) Jones, M.-C.; Leroux, J.-C. Polymeric micelles a new generation of colloidal drug carriers. *Eur. J. Pharm. Biopharm.* **1999**, *48* (2), 101−111.
(16) Zhu, Y.; Batchelor, R.; Lowe, A. B.; Roth, P. J. Design of thermoresponsive polymers with aqueous lcst, ucst, or both: Modification of a reactive poly(2-vinyl-4,4-dimethylazlactone) scaffold. *Macromolecules* **2016**, *49* (2), 672−680.
(17) Longenecker, R.; Mu, T.; Hanna, M.; Burke, N. A. D.; Stöver, H. D. H. Thermally responsive 2-hydroxyethyl methacrylate polymers: Soluble-insoluble and soluble-insoluble-soluble transitions. *Macromolecules* **2011**, *44* (22), 8962−8971.
(18) Mori, H.; Kato, I.; Saito, S.; Endo, T. Proline-based block copolymers displaying upper and lower critical solution temperatures. *Macromolecules* **2010**, *43* (3), 1289−1298.
(19) Kitazawa, Y.; Ueki, T.; McIntosh, L. D.; Tamura, S.; Niitsuma, K.; Imaizumi, S.; Lodge, T. P.; Watanabe, M. Hierarchical sol-gel transition induced by thermosensitive self-assembly of an abc triblock polymer in an ionic liquid. *Macromolecules* **2016**, *49* (4), 1414−1423.
(20) Mäkinen, L.; Varadharajan, D.; Tenhu, H.; Hietala, S. Triple hydrophilic ucstlcst block copolymers. *Macromolecules* **2016**, *49* (3), 986−993.
(21) Liang, X.; Liu, F.; Kozlovskaya, V.; Palchak, Z.; Kharlampieva, E. Thermoresponsive micelles from double lcst-poly (3-methyl-n-vinylcaprolactam) block copolymers for cancer therapy. *ACS Macro Lett.* **2015**, *4* (3), 308−311.
(22) Liu, F.; Kozlovskaya, V.; Medipelli, S.; Xue, B.; Ahmad, F.; Saeed, M.; Cropek, D.; Kharlampieva, E. Temperature-sensitive polymersomes for controlled delivery of anticancer drugs. *Chem. Mater.* **2015**, *27* (23), 7945−7956.
(23) Li, Z.; Tang, Y.-H.; Lei, H.; Caswell, B.; Karniadakis, G. E. Energy-conserving dissipative particle dynamics with temperature-dependent properties. *J. Comput. Phys.* **2014**, *265* (0), 113−127.
(24) Tang, Y.-H.; Karniadakis, G. E. Accelerating dissipative particle dynamics simulations on GPUs: Algorithms, numerics and applications. *Comput. Phys. Commun.* **2014**, *185* (11), 2809−2822. The source code is open under the GPLv3 license at http://www.cfm.brown.edu/repo/release/USER-MESO/.
(25) Li, Z.; Tang, Y.-H.; Li, X.; Karniadakis, G. E. Mesoscale modeling of phase transition dynamics of thermoresponsive polymers. *Chem. Commun.* **2015**, *51*, 11038−11040.
(26) Akkermans, R. L. C.; Briels, W. J. Coarse-grained dynamics of one chain in a polymer melt. *J. Chem. Phys.* **2000**, *113* (15), 6409−6422.
(27) Kinjo, T.; Hyodo, S. Equation of motion for coarse-grained simulation based on microscopic description. *Phys. Rev. E* **2007**, *75*, 051109.
(28) Hijon, C.; Espanol, P.; Vanden-Eijnden, E.; Delgado-Buscalioni, R. Mori-zwanzig formalism as a practical computational tool. *Faraday Discuss.* **2010**, *144*, 301−322.
(29) Li, Z.; Bian, X.; Caswell, B.; Karniadakis, G. E. Construction of dissipative particle dynamics models for complex fluids via the mori-zwanzig formulation. *Soft Matter* **2014**, *10* (43), 8659−8672.
(30) Li, Z.; Bian, X.; Li, X.; Karniadakis, G. E. Incorporation of memory effects in coarse-grained modeling via the mori-zwanzig formalism. *J. Chem. Phys.* **2015**, *143* (24), 243128.
(31) Li, Z.; Dormidontova, E. E. Kinetics of diblock copolymer micellization by dissipative particle dynamics. *Macromolecules* **2010**, *43* (7), 3521−3531.
(32) Gavrilov, A. A.; Chertovich, A. V.; Kramarenko, E. Yu. Conformational behavior of a single polyelectrolyte chain with bulky counterions. *Macromolecules* **2016**, *49* (3), 1103−1110.



DOI: 10.1021/acs.macromol.6b00365
*Macromolecules* 2016, 49, 2895−2903

(33) Groot, R. D.; Warren, P. B. Dissipative particle dynamics: Bridging the gap between atomistic and mesoscopic simulation. *J. Chem. Phys.* **1997**, *107*, 4423.
(34) Espanol, P.; Warren, P. Statistical mechanics of dissipative particle dynamics. *EPL (Europhys. Lett.)* **1995**, *30* (4), 191.
(35) Groot, R. D.; Rabone, K. L. Mesoscopic simulation of cell membrane damage, morphology change and rupture by nonionic surfactants. *Biophys. J.* **2001**, *81* (2), 725−736.
(36) Wu, C.; Zhou, S. Laser light scattering study of the phase transition of polyan-isopropylacrylamidea in water. 1. single chain. *Macromolecules* **1995**, *28* (24), 8381−8387.
(37) Rampf, F.; Paul, W.; Binder, K. On the first-order collapse transition of a three-dimensional, flexible homopolymer chain model. *EPL (Europhysics Letters)* **2005**, *70* (5), 628.
(38) Han, Y.; Yu, H.; Du, H.; Jiang, W. Effect of selective solvent addition rate on the pathways for spontaneous vesicle formation of aba amphiphilic triblock copolymers. *J. Am. Chem. Soc.* **2010**, *132* (3), 1144−1150.
(39) Simone, E.A.; Dziubla, T. D.; Muzykantov, V. R. Polymeric carriers: role of geometry in drug delivery. *Expert Opin. Drug Delivery* **2008**, *5* (12), 1283−1300.
(40) Wei, P.; Cook, T. R.; Yan, X.; Huang, F.; Stang, P. J. A discrete amphiphilic organoplatinum(ii) metallacycle with tunable lower critical solution temperature behavior. *J. Am. Chem. Soc.* **2014**, *136* (44), 15497−15500.
(41) Kim, S. D.; Kim, S. Y.; Chung, I. S. Unprecedented lower critical solution temperature behavior of polyimides in organic media. *Macromolecules* **2014**, *47* (24), 8846−8849.
(42) Nieh, M.-P.; Dolinar, P.; Kučerka, N.; Kline, S. R.; Debeer-Schmitt, L. M.; Littrell, K. C.; Katsaras, J. Formation of kinetically trapped nanoscopic unilamellar vesicles from metastable nanodiscs. *Langmuir* **2011**, *27* (23), 14308−14316.
(43) Arotçaréna, M.; Heise, B.; Ishaya, S.; Laschewsky, A. Switching the inside and the outside of aggregates of water-soluble block copolymers with double thermoresponsivity. *J. Am. Chem. Soc.* **2002**, *124* (14), 3787−3793.
(44) Contreras, F-X.; Sánchez-Magraner, L.; Alonso, A.; Goñi, F. M. Transbilayer (flip-flop) lipid motion and lipid scrambling in membranes. *FEBS Lett.* **2010**, *584* (9), 1779−1786.
(45) Fung, Y.-C. Stochastic flow in capillary blood vessels. *Microvasc. Res.* **1973**, *5* (1), 34−48.
(46) Bishop, J. J.; Popel, A. S.; Intaglietta, M.; Johnson, P. C. Effects of erythrocyte aggregation and venous network geometry on red blood cell axial migration. *Am. J. Physiol. Heart Circ. Physiol.* **2001**, *281* (2), H939−H950.
(47) Reinke, W.; Gaehtgens, P.; Johnson, P. C. Blood viscosity in small tubes: effect of shear rate, aggregation, and sedimentation. *Am. J. Physiol. Heart Circ. Physiol.* **1987**, *253* (3), H540−H547.
(48) Kim, S.; Kong, R. L.; Popel, A. S.; Intaglietta, M.; Johnson, P. C. Temporal and spatial variations of cell-free layer width in arterioles. *American Journal of Physiology-Heart and Circulatory Physiology* **2007**, *293* (3), H1526−H1535.
(49) Wang, D.; Yin, J.; Zhu, Z.; Ge, Z.; Liu, H.; Armes, S. P.; Liu, S. Micelle formation and inversion kinetics of a schizophrenic diblock copolymer. *Macromolecules* **2006**, *39* (21), 7378−7385.
(50) Liu, F.; Eisenberg, A. Preparation and ph triggered inversion of vesicles from poly aacrylic acida-b lock-polystyrene-b lock-poly (4-vinyl pyridine). *J. Am. Chem. Soc.* **2003**, *125* (49), 15059−15064.
(51) Hong, B.; Qiu, F.; Zhang, H.; Yang, Y. Dissipative particle dynamics simulations on inversion dynamics of spherical micelles. *J. Chem. Phys.* **2010**, *132* (24), 244901.
(52) Yong, X.; Kuksenok, O.; Matyjaszewski, K.; Balazs, A. C. Harnessing interfacially-active nanorods to regenerate severed polymer gels. *Nano Lett.* **2013**, *13* (12), 6269−6274.
(53) Chang, H.-Y.; Lin, Y.-L.; Sheng, Y.-J.; Tsao, H.-K. Multilayered polymersome formed by amphiphilic asymmetric macromolecular brushes. *Macromolecules* **2012**, *45* (11), 4778−4789.
(54) Wu, H.-L.; Sheng, Y.-J.; Tsao, H.-K. Phase behaviors and membrane properties of model liposomes: Temperature effect. *J. Chem. Phys.* **2014**, *141*, 124906.


DOI: 10.1021/acs.macromol.6b00365
*Macromolecules* 2016, 49, 2895−2903